JOURNAL OF AIRCRAFT
Vol. 35, No. 6, November–December 1998

Two-Dimensional Airfoil Performance Degradation Because of Simulated Freezing Drizzle

Russell Ashenden,* William Lindberg,† and John Marwitz‡
University of Wyoming, Laramie, Wyoming 82071

Wind-tunnel tests were conducted to determine the performance degradation of a scaled two-dimensional NACA 23012 airfoil (outboard wing section of the Wyoming King Air 200T) resulting from 1) ice because of various liquid hydrometeor sizes, 2) simulated drizzle ice roughness, and 3) simulated drizzle ice accretions on a model spar strap. The Wyoming King Air is equipped with a Saunders Fail-Safe Spar Strap that protrudes roughly 6 cm below the wing and extends spanwise from just outside both engine nacelles and may collect ice in large drop regions. The wind-tunnel evaluation facilitated quantifying the effects on aircraft performance degradation because of the King Air spar strap. The airfoil evaluations show that the drizzle drop ice shape and simulated drizzle ice roughness resulted in the highest performance degradation. In general, the ice shapes and simulated freezing drizzle roughness increased profile drag, reduced angle of attack for maximum lift coefficient, reduced the maximum lift coefficient, altered the pitching moment, reduced lift over drag ratio, and marginally changed the lift curve slope. These evaluations also show that the most sensitive surface location on an airfoil is on the suction side between 6 and at least 11% of chord. Ice contaminations in this area are beyond the protective de-icing boots of most aircraft and lead to severe degradations in lift and drag characteristics. In addition, these results suggest that an ice-contaminated spar strap will increase King Air drag by approximately 12% at angles of attack consistent with cruise. Furthermore, any ice that forms on the lower surface of the wing, forward of the spar strap, does not significantly increase profile drag.

Introduction

DIFFERENT aircraft responses in supercooled large drop (SLD) regions have been reported by Ashenden and Marwitz,[1,2] where they showed high rates of aircraft performance degradation in freezing drizzle (30–400 μm diameter) and low rates of performance degradation in icing conditions caused by cloud drops (<40 μm diameter) and freezing rain (>400 μm diameter). To examine these conditions closer, wind-tunnel tests were conducted in two phases to determine the performance degradation of a scaled two-dimensional NACA 23012 airfoil (outboard wing section of the Wyoming King Air). The first phase of this research consisted of evaluating the airfoil degradation as a result of ice caused by various liquid hydrometeor sizes. An ice accretion code was used to predict ice shapes using natural hydrometeor distributions obtained by the King Air during weather research flights. The simulated ice shapes evaluated were predicted for cloud, drizzle, and rain-sized liquid hydrometeors. This first phase of the wind-tunnel research was published by Ashenden et al.[3] Additional wind-tunnel evaluations were conducted during the second phase of this research to build upon the contributions of Ashenden et al. and they are presented here. The second phase evaluated airfoil performance degradation due to simulated drizzle ice roughness and simulated drizzle ice accretions on a model spar strap. A strip of 20-grit sandpaper was applied to the model to simulate ice roughness elements observed on the King Air during freezing drizzle encounters.[1] The model spar strap was a simulation of the full-scale Saunders Fail-Safe Spar Strap located on the lower surface of the King Air wing. The spar strap passes through the wheel wells and beneath the two engine nacelles and may collect ice in the large drop regions.[4,5] The simulated spar strap tests were included in the wind-tunnel evaluations in an effort to quantify the overall effects on the King Air performance degradation because of spar strap drizzle ice accretions.

Received Feb. 23, 1998; revision received May 20, 1998; accepted for publication May 21, 1998.

*Aircraft Icing Researcher, Ph.D., College of Engineering, Department of Atmospheric Science.

†Professor, College of Engineering, Mechanical Engineering Department.

§Professor, College of Engineering, Department of Atmospheric Science.

Model Configurations

Thirteen model configurations evaluated in the wind tunnel are listed in Table 1. These included a clean airfoil baseline, simulated ice shapes (from Ashenden et al.[3]), a simulated spar strap, the spar strap with simulated drizzle ice accretion, 20-grit roughness strips and, combinations thereof. The simulated ice shapes were predicted using the NASA Lewis Research Center LEWICE 1.6 computer code.[6] This is a two-dimensional ice accretion code that applies a time-stepping procedure to calculate the shape of an ice accretion. LEWICE is considered a research code and its applicability in the large drop, near-freezing regime has been questioned; however, LEWICE 1.6 incorporates improvements in this area. These improvements include numerical modifications allowing for a large number of time steps and an empirically based roughness model. Other areas of concern are drop splashing and ice shedding, which were not considered during the ice prediction runs. Considering these concerns, LEWICE 1.6 may only provide a rough estimate of the ice shape and location prior to shedding and sliding. The details of the ice shape prediction and fabrication are discussed by Ashenden et al.[3] The ice shapes predicted are shown for the NACA 23012 airfoil in Fig. 1. All input parameters were identical for the various shapes, with the exception of drop distributions; therefore, the resultant ice shape variations were a result of drop-size variations alone. Note that the main difference between the shapes shown in Fig. 1 is impingement limits, or maximum chordwise extent. The resulting ice shapes, with varying chord extent and identical surface roughness, provided test articles that provided insight into the effects of airfoil performance and aerodynamic degradation from varying impingement limits.

Table 1 Model configurations

Run	Configuration	Description
1	Clean	NACA 23012 baseline
2	Cloud Shape	Ice shape, 20 μm mono-dispersed
3	Drizzle Shape	Ice shape, freezing drizzle distribution
4	Rain Shape	Ice shape, freezing rain distribution
5	R* Drizzle Shape	Residual drizzle ice shape, after boot
6	R* Rain Shape	Residual rain ice shape, after boot
7	Spar	Spar strap applied to lower surface
8	Spar, Ice	Spar strap, ice on leading edge of strap
9	Spar, 20*L*	Spar strap, 20 grit on lower surface
10	Spar, 20*U*	Spar strap, 20 grit on upper surface
11	Spar, 20*UL*	Spar strap, 20 grit on upper and lower
12	Spar, 20*ULI*	Spar strap, 20 grit on upper and lower, ice on leading edge of strap
13	30*U*	20 grit on upper surface

Note: Runs 1–6 from Ashenden et al.[3]

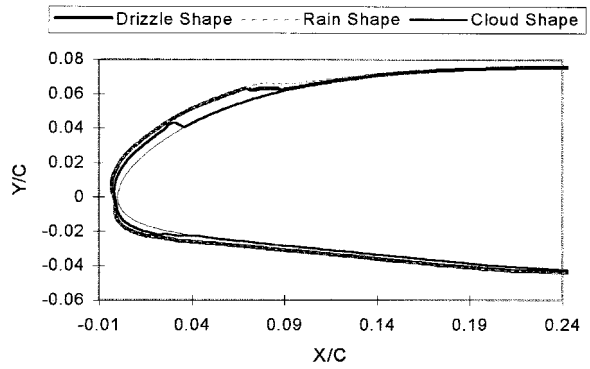

Fig. 1 NACA 23012 airfoil predicted cloud, drizzle, and rain drop ice shapes. *Y/C* and *X/C* represent chord normalized airfoil coordinates. The LEWICE inputs consisted of liquid water content = 0.36 g/m^3, temperature = 270.15 K, *V* = 80 m/s, α = 2.0 deg, airfoil chord = 1 m, and 15 min simulated icing exposure. Figure taken from Ashenden et al.[3]

The Saunders Fail-Safe Spar Strap consists of a stainless-steel strap that connects the inboard segment of the outer wing panels along the lower surface. The simulated spar strap was fabricated from balsa wood, smoothed with epoxy, and applied to the lower surface of the model shown in Fig. 2. The full-scale spar strap varies spanwise in height and width, where it protrudes approximately 6 cm below the fuselage and decreases to zero just outboard of the engine nacelles, resulting in a spanwise coverage of approximately 50% of the total wingspan. The geometry of the strap for an inboard wing location was selected because the wind-tunnel evaluation is two dimensional. Figure 3 shows the ice that can accumulate on the leading edge of the spar strap when encountering drizzle-sized drops. The height of the visible ice ridge is approximately 5 cm. This photograph was taken after landing, so that it can be assumed that the ice ridge could have been larger during flight. To evaluate the aerodynamic effects of accumulated ice on the spar strap, a bead of silicon caulk was added to the model as shown in Fig. 4. The height of the ice ridge tested corresponded to a height of approximately 5 cm (k/c = 0.0215) for a wing chord of 2.18 m.

Observations by the King Air flight crew suggest that the drizzle drops freeze as sharp feathers or glaze nodules at or just beyond the de-icing boots as shown in Fig. 5.[1] The King Air performance recovery in ice crystals discussed by Ashenden and Marwitz[2] suggests that the sharpness of the ice nodules may affect the level of aerodynamic degradation. Because the ice shape evaluations (phase I) normalized surface roughness, a roughness test was included in the phase II wind-tunnel tests to evaluate the aerodynamic effects of the sharp roughness elements observed in flight. This evaluation consisted of adding 3M™ 20-grit sandpaper to the airfoil in spanwise strips.

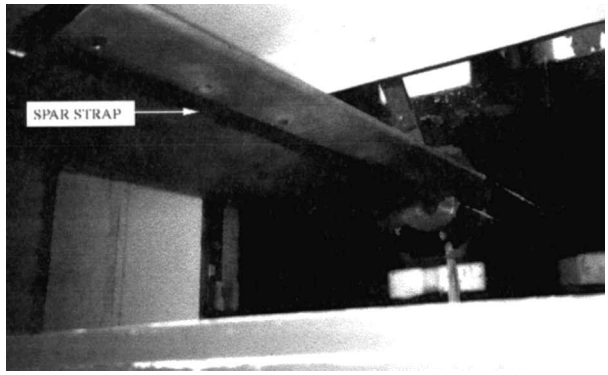

Fig. 2 NACA 23012 airfoil model (0.203-m chord) with simulated spar strap applied to lower surface.

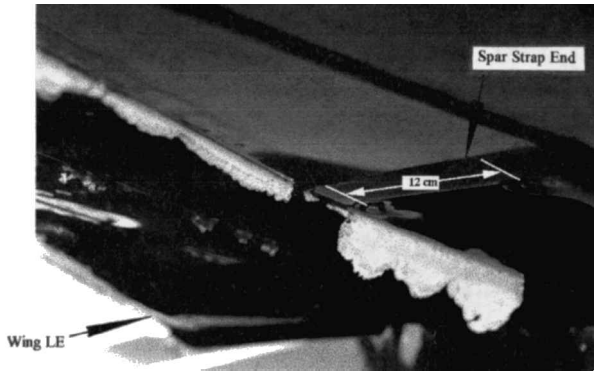

Fig. 3 Ice accretion on leading edge (LE) of the left, outboard portion of the King Air spar strap remaining after landing. Foreground bolt hole spacing is 12 cm for scaling reference.

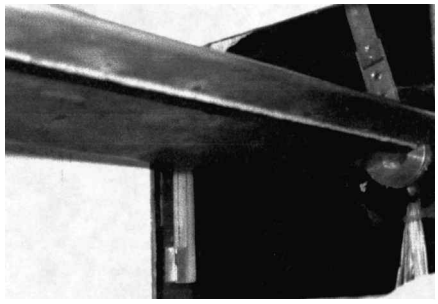

Fig. 4 NACA 23012 airfoil model (0.203-m chord) and simulated spar strap with bead of silicon caulk to simulate observed ice accretions.

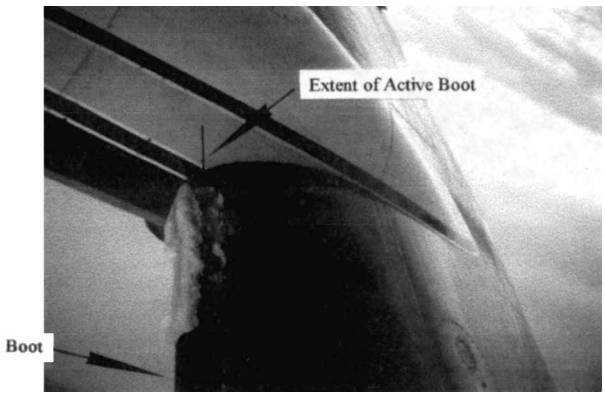

Fig. 5 Drizzle ice accretion on right wing of King Air. The inboard portion of the wing between the fuselage and the nacelle is shown. The chordwise extent of the pneumatic boot is indicated.

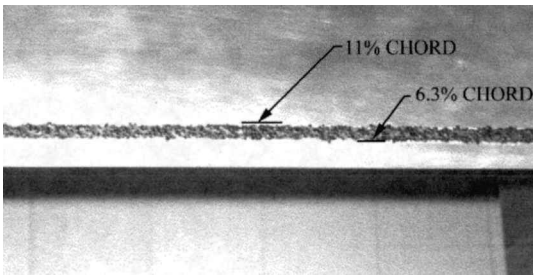

Fig. 6 NACA 23012 airfoil model (0.203 m chord) with 20-grit sandpaper applied to the upper surface in a spanwise strip. The roughness strip extends from 6.3 to 11% of wing chord.

The 10.3-mm-width strips extended from 6.3 to 11% of wing chord with corresponding roughness element heights of 17 mm (k/c = 0.0078) for a wing chord of 2.18 m. A strip was either applied to the upper surface (20U), the lower surface (20L) or both surfaces (20UL). A roughness strip was applied to the upper airfoil surface in Fig. 6.

Description of Test Facility, Instrumentation, and Model

The two-dimensional airfoil icing evaluation was conducted using the Wyoming Low Speed Wind Tunnel.[3,7] Plexiglas® doors are mounted on both sides of the 2 × 2 × 3 ft test section to ease access and provide model viewing. The test model is mounted horizontally in the test section and is linked to a protractor via a lever-arm that is pinned at the desired angle of attack, α. The indicated α, therefore, is geometrically derived and does not account for upwash effects. The open-circuit tunnel Reynolds number operating range was 3.4 to 5.9 × 10^5, based on the 0.203-m (8.0-in.) model chord. Tunnel velocity fluctuations resulting from turbulence and fan unsteadiness were less than 1%.

A pitot-static probe mounted 1.5 chord lengths forward of the test model and connected to an Omega™ transducer was used to measure test section dynamic pressure. The transducer was calibrated using a U-tube water manometer for the full speed range of the tunnel. Calibrations were repeated throughout the evaluations to check accuracy. The airfoil pressure ports were connected to a scanning system that consisted of a selectable valve and the Omega transducer. The pressure from each airfoil port, referenced to upstream static pressure, was recorded by a personal computer based data logging system. Each port was scanned for 30 s at a frequency of 10 Hz, resulting in 300 data points per port for each α. These points were averaged to provide a steady-state value. The same transducer was used to measure the dynamic pressure from the traversing pitot-tube used during wake deficit measurements.

The wind-tunnel model used in this evaluation was a single-element, 0.203-m chord, pressure instrumented, polished aluminum NACA 23012 airfoil that spanned the full width of the test section. This model represents a 20% mean chord section of the Wyoming King Air outboard wing. There are a total of 23 pressure ports distributed along the chord of the airfoil: 12 ports on the upper surface, 10 on the lower surface, and 1 at the leading edge. These ports were placed in a chevron pattern along the airfoil centerline for minimal tap and wall effects. A complete description of the NACA 23012 model fabrication was detailed by Hoxie.[7]

Test Procedures and Results

The NACA 23012 airfoil was mounted horizontally in the test section with a traversing pitot-probe mounted two chord lengths downstream of the airfoil trailing edge. Airfoil pressure coefficients and wake deficit data were obtained for the NACA 23012 airfoil for the 13 configurations listed in Table 1 for angles of attack from −2 to 18 deg. Tunnel runs 1–6 are from Ashenden et al.[3] The residual drizzle and residual rain drop ice shapes represented the ice remaining on the airfoil after a simulated boot activation. The ice shapes were removed to the 6.3% chord position resulting in severe ridges, or steps, on both the upper and lower surfaces as shown in Fig. 2 of Ashenden et al.[3] It was assumed that a simulated boot activation with the cloud drop ice shape would remove all appreciable ice, so this procedure was not performed with the cloud drop ice shape. The performance degradation as a result of the remaining ridges was considered a worst-case scenario because no ice was removed aft of the 6.3% chord ridge. Realistically, some of this ice would slide aft or shed after a boot activation. At the completion of the ice shape evaluations, the model was stripped and a baseline run was completed prior to adding the spar strap and subsequent configurations.

A sweep of angles of attack was made for each configuration, while recording the upstream and airfoil static pressures. The test section was then traversed with the trailing pitot-static probe at each α to measure the wake deficit. Using the free-stream dynamic pressure, the model static pressures were converted to pressure coefficients, C_p, and integrated to provide sectional lift, C_L, and pitching moment, $C_{mc/4}$, coefficients for each test configuration, and α as described by Rae and Pope.[8] The wake momentum deficit measured by the trailing pitot-probe was integrated to determine drag coefficients, C_D, for each configuration and α. The tunnel velocity was approximately 50 m/s, which corresponds to a Reynolds number of 5.5 × 10^5 for the 0.203-m model. The uncertainties in calculating C_L and C_D are discussed by Ashenden[9] and are provided in columns two and three in Table 2.

Clean Airfoil

The observed clean airfoil stall angle varied between 16 and 18 deg, depending on how slowly the higher angles were approached; however, no flow separations occurred below 16 deg. The clean airfoil maximum lift coefficient, or $C_{L\max}$, was 1.393 at α = 16 deg.[3]

The clean airfoil C_D compared favorably to the standard roughness data set provided by Abbott and Von Doenhoff.[10] The model utilized during this evaluation incorporated recessed screw holes (filled with wax) on the lower surface, possibly explaining the similarity to the standard roughness drag. The drag coefficients were nearly identical up to a C_L corresponding to α = 6 deg. The lift and drag results for the clean airfoil established a satisfactory baseline to proceed with the remaining configurations.

Simulated Ice Shape Evaluations

Airfoil pressure coefficients and wake deficit data were obtained by Ashenden et al.[3] for the NACA 23012 airfoil with the addition of the ice shapes listed in Table 1 from α = 0 to 16 deg. Comparisons of C_L and C_D were taken from Ashenden

Table 2 NACA 23012 sectional lift and drag comparison for tunnel runs

α, deg	Clean airfoil		% C_L change/% C_D change from clean airfoil				
	C_L	$C_D \pm 7\%$	Cloud	Drizzle	Rain	R^* drizzle	R^* rain
−2	−0.023 ± 0.022	0.01	−66/6	50/49	ND	ND/+140	ND/+100
0	0.163 ± 0.033	0.009	15/11	16/55	19/42	−15/ND	ND
2	0.389 ± 0.031	0.01	−1/7	−4/56	5/35	−16/450	ND/+240
4	0.665 ± 0.033	0.011	−12/14	−14/56	−14/26	ND	ND
6	0.879 ± 0.025	0.013	−10/16	−6/51	−7/23	−26/790	−22/590
8	1.034 ± 0.039	0.016	−8/30	−6/53	−4/15	−32/ND	−22/ND
10	1.241 ± 0.038	0.019	−16/36	−8/49	−8/10	−44/ND	−23/ND
12	1.327 ± 0.050	ND	−17/ND	−6/ND	−8/ND	−50/ND	−32/ND
13	1.339 ± 0.048	ND	−35/ND	−43/ND	−8/ND	ND	ND
14	1.371 ± 0.047	ND	−38/ND	−42/ND	−42/ND	−47/ND	−34/ND
16	1.393 ± 0.048	ND	ND	ND	−39/ND	ND	ND

Note: From Ashenden et al.,[3] $Re = 5.5 \times 10^5$, ND = no data obtained, R^* = residual ice shape.

et al. and are provided in Table 2 with the noted measurement uncertainty.[9] The five ice simulation tests were compared to the clean baseline test to determine the NACA 23012 airfoil performance and aerodynamic degradation. The cloud drop ice shape at α = 12 deg resulted in the highest $C_{L\max}$ reduction of 21% when excluding the residual ice shapes.[3] This configuration, however, resulted in the lowest drag coefficients at the lower angles of attack. The high C_L change because of the cloud drop ice shape is not surprising considering that the leading edge is the most sensitive to contamination effects. The cloud drop ice shape is also the easiest to remove in an actual boot activation because of the limited ice extent from the leading edge.

The drizzle and rain drop ice shapes resulted in similar coefficients of maximum lift of approximately 1.2 (reduction of 11%); however, the corresponding angles of attack were α = 12 deg for the drizzle and α = 13 deg for the rain drop ice shape.[3] As mentioned earlier, the main differences between the drizzle and rain drop ice shapes were impingement limits. These results indicate that the rain drop ice shape, with the larger impingement limits, may retard flow separation (or delay stall). Both the drizzle and rain drop ice shapes resulted in positive pitching moment coefficients (nose up), with the drizzle drop ice shape causing the highest increase.[3] This positive trend was different from the cloud and residual ice shapes, which experienced negative decreases. As shown in Table 2, the drizzle ice shape C_D increase was on the order of 50% for all angles tested. The rain drop ice shape drag coefficients behave differently when compared with the cloud and drizzle drop ice shapes. The highest rain drop ice shape C_D increase was 42% at α = 0 deg, decreasing to 10% at α = 10 deg. This drag phenomena resulted in lower rain drop ice shape drag coefficients at the higher angles when compared to the cloud and drizzle drop ice shapes.

The residual drizzle and residual rain ice shapes simulated the remaining ice aft of the de-icing boot after an activation. These shapes resulted in the highest reductions in C_L, the highest changes to $C_{mc/4}$, and the highest increases in C_D (790 and 590% at α = 6 deg). The residual drizzle and rain drop ice shape $C_{L\max}$ decreased by 50 and 34%, respectively.[3] The simulated boot activation was a worst-case scenario because the ice was predicted using a 15-min exposure, with the assumption that no ice shed or slid back on the airfoil. In an actual aircraft icing situation, the pilot may cycle the boots within the 15-min exposure and some of the ice aft of the boots would shed or slide aft possibly reducing its negative effect on lift, drag, and pitching moment. These actions, however, are not guaranteed and the results presented herein provide some insight on what to expect if the boots are cycled late and a minimal amount of ice sheds or slides aft. In addition, researchers have shown that cycling the de-icing boots after a freezing drizzle encounter may result in no noticeable benefit to aircraft performance.[2] The observed performance degradation from the various ice shapes are because of ice-shape geometry and impingement limit variations alone. The surface roughness for all simulated ice shapes was identical and, therefore, not a factor when evaluating the airfoil performance degradation. In actuality, the surface roughness for the three ice shapes would vary substantially. Anecdotal evidence from the Wyoming King Air flight crews suggests that the ice formed by freezing drizzle is very rough and the ice formed by freezing rain is smooth and conformal.[1] This freezing drizzle surface roughness characteristic could lead to an even higher airfoil performance degradation. Surface roughness, however, may help retard flow separation in certain situations. As mentioned earlier, the rain drop ice shape, with the larger impingement limits, had a higher stall angle (delayed flow separation). This delayed separation may have been a result of the increased roughness beyond the maximum wing thickness and/or, possibly, because of the more gradual ice to airfoil transition step compared to the drizzle ice shape. To evaluate the rough drizzle ice observed by the flight crews, the simulated ice roughness configurations were added to the wind-tunnel evaluations.

Airfoil Spar Strap and Simulated Drizzle Ice Roughness Evaluations

Airfoil pressure coefficients and wake deficit data were obtained for the NACA 23012 airfoil with the addition of the simulated spar strap and the roughness configurations listed in Table 1 for α = −2 to 20 deg. The corresponding lift curve slopes, quarter-chord pitching moment coefficients, and drag polars are in Figs. 7, 8, and 9, respectively. Comparisons of C_L and C_D along with lift over drag ratios, L/D, are provided in Table 3. These configurations were compared to the clean airfoil test to determine the NACA 23012 airfoil aerodynamic degradation. A comparison between the Spar and Spar Ice configurations in Table 3 shows that the ice-contaminated spar strap results in a C_D increase of 12% at α = 6 deg. This α corresponds to the King Air inboard wing α during cruise (wing root incidence plus α). The highest $C_{L\max}$ reduction was 30% with the Spar 20*ULI* configuration (spar strap with ice and 20 grit on upper and lower surface) at α = 10 deg. This configuration resulted in a high positive pitching moment at α = 8 deg and a high negative moment at α = 12 deg as depicted in Fig. 8. The Spar 20*ULI* configuration also resulted in the highest drag coefficients shown in Fig. 9 (C_D increased 172% at α = −2 deg). The L/D plot in Fig. 10 normalizes the drag increase associated with increasing α. The Spar 20*ULI* results in the lowest L/D (~66% decrease) for all angles tested and is, therefore, the configuration with the highest performance degradation. The Spar 20UL and Spar 20U configurations resulted in the next highest performance degradations with reductions in $C_{L\max}$ near 30% at α = 10 deg, C_D increased 120% at α = 6 deg, and reductions in L/D near 65%. The pitching moments behaved similarly to the Spar 20*ULI* configuration. The third highest degradation occurred when only the 20-grit sandpaper was applied to the upper surface (no spar strap).

Table 3 Coefficient comparison for NACA 23012 airfoil (spar strap and roughness added)

α, deg	Spar			Spar + ice			Spar + 20*L*			Spar + 20*U*			Spar + 20*UL*			Spar + 20*ULI*			20*U*		
	C_L	C_D	*L/D*	C_L	C_D	*L/D*	C_L	C_D	*L/D*	C_L	C_D	*L/D*	C_L	C_D	*L/D*	C_L	C_D	*L/D*	C_L	C_D	*L/D*
−2	24	65	54	236	117	163	93	81	96	ND	ND	ND	−330	118	−97	−330	172	−58	ND	ND	ND
0	4	47	−29	30	97	−34	0	70	−41	−26	117	−66	−26	132	−68	−23	165	−71	−26	53	−52
2	−2	26	−22	10	73	−36	−2	46	−32	−20	107	−61	−20	134	−66	−14	144	−65	−15	69	−50
4	−7	28	−28	−3	66	−41	−10	40	−35	−22	112	−63	−24	125	−66	−21	143	−68	−15	89	−55
6	−5	29	−26	−4	41	−32	−3	37	−30	−21	117	−64	−21	120	−64	−20	141	−67	−15	98	−57
8	ND	ND	ND	−3	31	−26	−2	31	−25	−19	131	−65	−19	134	−65	−20	137	−66	−15	ND	ND
10	16	19	−22	−3	28	−24	−3	17	−17	−29	ND	ND	−30	141	−71	−30	143	−71	−26	ND	ND
12	ND	ND	ND	ND	ND	ND	−3	ND	ND	−38	ND	ND	−39	ND	ND	−40	ND	ND	−36	ND	ND
14	ND	ND	ND	ND	ND	ND	ND	ND	ND	−49	ND	ND	ND	ND	ND	ND	ND	ND	−47	ND	ND

Notes: Re = 5.5 × 10^5, ND = No Data Obtained.

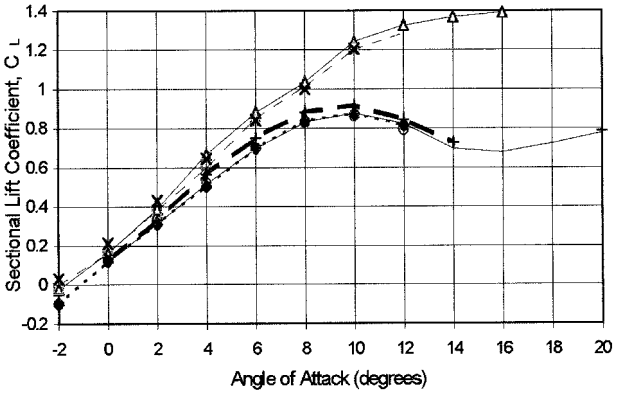

Fig. 7 C_L for clean NACA 23012 airfoil measured (△) and with addition of the spar strap (□), Spar with 20*L* (---), Spar with 20U (——), Spar with 20*UL* (♦), Spar with Ice (×), Spar with 20*ULI* (○), and 20*U* (– – –). The clean $C_{L\max}$ corresponds to α = 16 deg. The Spar 20*U*, Spar 20*UL*, Spar 20*ULI*, and 20*U* $C_{L\max}$ correspond to α = 10 deg. Wind-tunnel *Re* = 5.5 × 10^5.

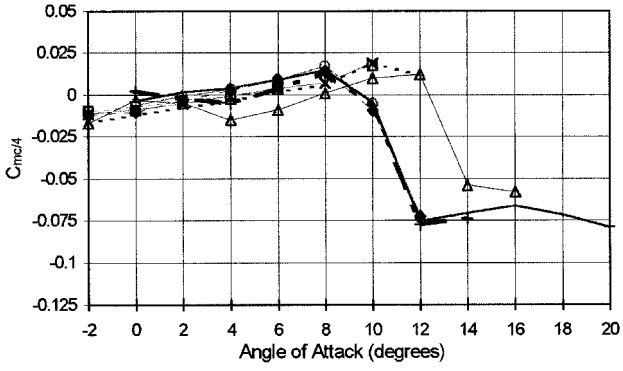

Fig. 8 $C_{mc/4}$ for clean NACA 23012 airfoil (△) and with addition of the spar strap (□), Spar with 20*L* (---), Spar with 20*U* (——), Spar with 20*UL* (♦), Spar with ice (×), Spar with 20*ULI* (○), and 20*U* (– – –).

This configuration, 20*U*, resulted in a 26% reduction in $C_{L\max}$ at α = 10 deg, a C_D increase of 98% at α = 6 deg, a *L/D* reduction near 55%, and similar pitching moment characteristics to the 20*ULI* configuration. The sensitivity of the upper surface of the airfoil to roughness is apparent in the results of the 20*U* evaluation.

Compared with the upper surface, the effect of adding configurations to the lower surface of the airfoil was not as severe. For example, C_D increased between 19 and 65%, C_L decreased 5% at α = 6 deg, and *L/D* decreased 26% with the addition of the spar strap (Spar). When the simulated ice was added to the leading edge of the spar strap, C_D increased 73% at α = 2 deg and 28% at α = 10 deg. The effect on lift was significant at α = −2 deg, but minor at the higher angles (4% C_L reduction at α = 6 deg). *L/D* decreased by 32% at α = 6 deg because

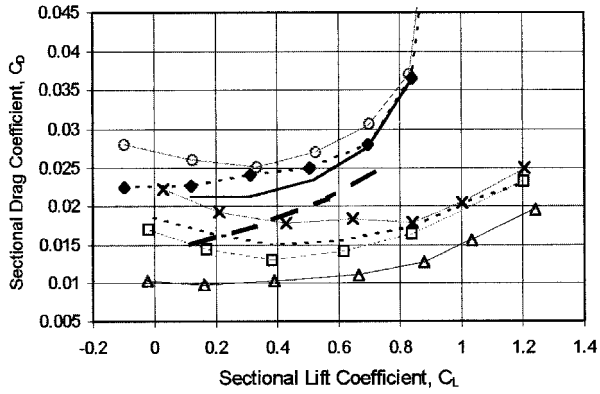

Fig. 9 Drag Polars for clean NACA 23012 airfoil (△) and with addition of the spar strap (□), Spar with 20*L* (---), Spar with 20*U* (——), Spar with 20*UL* (♦), Spar with Ice (×), Spar with 20*ULI* (○), and 20*U* (– – –).

of the increase in profile drag. As shown in Fig. 9, the effect of adding the 20-grit sandpaper to the lower surface (Spar 20*L*) was more pronounced at the lower angles of attack. The drag polar approached the spar strap configuration when α was increased. The C_D increased 46% at α = 2 deg and 17% at α = 10 deg. C_L and $C_{mc/4}$ for the Spar 20L configuration were similar to the spar strap case with slightly lower *L/D* values (30% *L/D* reduction at α = 6 deg) because of the increased profile drag.

A review of Figs. 7–10 and Table 3 illustrates that the effect of adding a spar strap and simulated drizzle ice to the lower surface of a clean airfoil modifies C_L insignificantly, slightly modifies $C_{mc/4}$, moderately increases C_D, and moderately reduces *L/D* (31% at α = 8 deg). The largest concern here is the increase in C_D, such as the 73% increase at α = 2 deg. Considering a full-scale aircraft (*Re* = 2.7 to 5.9 × 10^6), such as the King Air, this drag increase is significant but not catastrophic based on available engine thrust. The effect of adding simulated drizzle ice to the upper surface, however, is of greater concern. The upper surface configurations decrease C_L significantly (~30% at α = 10 deg), significantly modifies $C_{mc/4}$, significantly increases C_D (107% at α = 2 deg) and substantially reduces *L/D* (~65% at α = 8 deg). As shown in Fig. 7, the effect of upper surface roughness is to change the zero lift α, reduce the lift curve slope, reduce $C_{L\max}$, and trigger thin airfoil stall. That is, roughness elements on the upper wing surface decreases lift and increases stall speed in addition to increasing profile drag significantly. Again, this evaluation applied roughness between 6 and 11% of chord; however, other researchers,[11–13] have shown that this sensitive location may extend back to approximately 15% of chord. Furthermore, the wind-tunnel work of Calay et al.[11] was accomplished at a Reynolds number of 1.25 × 10^6 (the same magnitude as full-scale King Air) and essentially reached the same conclusions as presented here. The fact that Calay et al. determined that ice shapes at 5 and 15% of chord were more detrimental to C_L

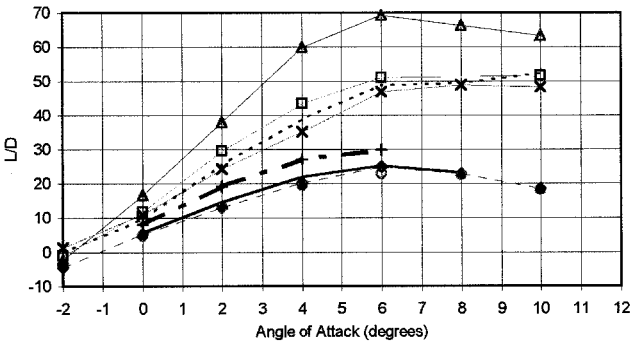

Fig. 10 *L/D* for clean NACA 23012 airfoil measured (△) and with addition of the spar strap (□), Spar with 20*L* (---), Spar with 20*U* (——), Spar with 20*UL* (♦), Spar with Ice (×), Spar with 20*ULI* (○), and 20*U* (– – –). Highest aerodynamic degradation corresponds to lowest *L/D* values.

and C_D compared with shapes at 25% of chord substantiates the work presented here accomplished at a Reynolds number of 5.5×10^5.

The results presented herein and by Ashenden et al.[3] support the performance degradation of the Wyoming King Air when encountering freezing drizzle and rain. As discussed earlier, the King Air experiences the highest performance degradation in freezing drizzle. The same trends are illustrated in the wind-tunnel results with the highest airfoil degradation occurring with the drizzle drop ice shape and the simulated drizzle ice roughness applied to the upper surface. The results in Ashenden and Marwitz[1] show the degradation to be more severe in the freezing drizzle environment than found in the wind tunnel. For example, the Jan. 18, 1983[1] drizzle case experienced a maximum C_D corresponding to an increase of over 200%, whereas, the wind-tunnel evaluation for the sectional airfoil showed an increase on the order of 50% for the simulated drizzle drop ice shape and 140% for the simulated drizzle roughness (Spar 20*ULI*). The higher degradation for the aircraft can be explained by the addition of other aircraft components such as the fuselage, tail, and the many ice collectors protruding from the aircraft (instrumentation pylons, particle decelerator). In addition, the effects of residual ice ridges and surface roughness may have contributed to the large increase in King Air drag. The possibility exists that residual ice ridges on the King Air provided the increase in drag, similar to that found for the residual ice shapes in the wind tunnel. In addition, rough ice formed by freezing drizzle on other surfaces of the aircraft may have amplified the King Air performance degradations.

The contaminated model $C_{L\max}$ closely corresponds to the α, at which the King Air experiences aerodynamic buffet. The King Air experiences buffet when approaching stall, or perhaps, near aircraft $C_{L\max}$. During icing encounters in freezing drizzle, the King Air flight crews have experienced buffet when the indicated α approached 6 deg.[1] The inboard portion of the wing α is approximately 10 deg, when the aircraft α indicates 6.5 deg, because this portion of the wing has an incidence of 3.5 deg. For comparison, the $C_{L\max}$ for the NACA 23012 corresponded to $\alpha = 10$ deg when the simulated drizzle ice roughness was applied to the upper surface. Airflow separating near the leading edge of the inboard portion of the wing results in aerodynamic buffet during freezing drizzle encounters. An increase in α beyond 10 deg would typically cause increased flow separations, possibly catastrophic separation for a wing with no twist. Fortunately, twist was designed into the wing and the outboard portion of the wing will typically stall after the inboard portion because of a lower incidence (approximately -1 deg at wing tip). This King Air characteristic maintains lateral control via the ailerons located on the outboard section of the wings. This design fortuitously allows the flight crews to fly to buffet for performance degradation monitoring.

Summary

Generally, the configurations listed in Table 1 increased C_D, reduced α for $C_{L\max}$, reduced $C_{L\max}$, altered $C_{mc/4}$, reduced L/D, and marginally changed the lift curve slope. The main aerodynamic effects because of ice shapes were an early flow separation and a change in $C_{mc/4}$.[3] The ice shape results show that prior to boot activation the cloud drop ice shape has the highest C_L degradation and the drizzle drop ice shape has the highest C_D increase. After boot activation, the drizzle drop ice shape has the highest C_L and C_D performance degradation and the highest aerodynamic degradation as shown by the negative $C_{mc/4}$.

The wind-tunnel results suggest that the Saunders Fail-Safe Spar Strap will minimally increase King Air drag (12% at $\alpha = 6$ deg) when ice accretes on the leading portion of the spar strap. Furthermore, any ice that forms on the lower surface of the wing, forward of the spar strap, is not as effective in increasing profile drag with the spar strap installed. It is hypothesized that the spar strap leads to a thickening of the momentum boundary layer over the height of the roughness elements, therefore, these elements contribute very little to the overall profile drag. The effect of adding the simulated drizzle ice to the upper surface is high aerodynamic degradation (with or without the spar strap). These configurations led to the highest C_L decreases, the highest C_D increases, the highest L/D decreases, and the highest $C_{mc/4}$ variations. The ice that forms on the upper surface of the wing, as shown in Fig. 5, is similar to the configurations evaluated in the wind tunnel, which led to the highest degradations. These ice accretions on the King Air lead to aerodynamic buffet near an α corresponding to $C_{L\max}$ for the ice-contaminated two-dimensional model. These results show that the portion of the wing most sensitive to aerodynamic degradation is the upper surface between 6 and at least 11% of chord.

Acknowledgments

This research was funded by the Wyoming Planetary and Space Science Center, NASA Grant NGT 40050, and the Winter Icing and Storms Project, NSF Grant ATM-9523434. The Wyoming King Air was provided through a cooperative agreement between the University of Wyoming and the National Science Foundation, ATM-9319141. The authors thank Robert D. Kelly, Alfred R. Rodi, and Dudley E. Smith for their guidance and assistance.

References

[1]Ashenden, R., and Marwitz, J., "Turboprop Aircraft Performance Response to Various Environmental Conditions," *Journal of Aircraft*, Vol. 34, No. 3, 1997, pp. 278–287.

[2]Ashenden, R., and Marwitz, J., "Characterizing the Supercooled Large Droplet Environment with Corresponding Turboprop Aircraft Response," *Journal of Aircraft*, Vol. 35, No. 6, 1998, pp. 912–920.

[3]Ashenden, R., Lindberg, W., Marwitz, J., and Hoxie, B., "Airfoil Performance Degradation by Supercooled Cloud, Drizzle, and Rain Drop Icing," *Journal of Aircraft*, Vol. 33, No. 6, 1996, pp. 1040–1046.

[4]Cooper, W. A., Sand, W. R., Politovich, M. K., and Veal, D. L., "Effects of Icing on Performance of a Research Airplane," *Journal of Aircraft*, Vol. 21, No. 9, 1984, pp. 708–715.

[5]Sand, W. R., Cooper, W. A., Politovich, M. K., and Veal, D. L., "Icing Conditions Encountered by a Research Aircraft," *Journal of Climate and Applied Meteorology*, Vol. 23, Oct. 1984, pp. 1427–1440.

[6]Wright, W. B., "Users Manual for the Improved NASA Lewis Ice Accretion Code LEWICE 1.6," NASA Lewis Research Center, NASA CR 198355, Cleveland, OH, July 1995.

[7]Hoxie, B., "Experimental Study of the Effect of Ice Accretion on Wing Performance. Research Experiences in Fluid Mechanics," Department of Mechanical Engineering, Univ. of Wyoming, Laramie, WY, Aug. 1995.

[8]Rae, W. H., and Pope, A., *Low Speed Wind Tunnel Testing*, 2nd

ed., Wiley, New York, 1984, pp. 213–222.

[9]Ashenden, R., "Airfoil Performance Degradation by Supercooled Cloud, Drizzle, and Rain Drop Icing," M.S. Thesis, Dept. of Atmospheric Science, Univ. of Wyoming, Laramie, WY, 1996.

[10]Abbott, I. H., and Von Doenhoff, A. E., *Theory of Wing Sections Including a Summary of Airfoil Data*, Dover, New York, 1959.

[11]Calay, R. K., Holdø, A. E., Mayman, P., and Lun, I., "Experimental Simulation of Runback Ice," *Journal of Aircraft*, Vol. 34, No. 2, 1997, pp. 206–212.

[12]Bragg, M. B., "Aerodynamics of Supercooled-Large-Droplet Ice Accretions and the Effect on Aircraft Control," *Proceedings of the FAA International Conference on Aircraft Inflight Icing* (Springfield, VA), DOT/FAA/AR-96/81, II, 1996, pp. 387–399.

[13]Mullins, B. R., Smith, D. E., and Korkan, K. D., "Effects of Icing on the Aerodynamics of a Flapped Airfoil," AIAA Paper 95-0449, Jan. 1995.